A Spiral-like Acquisition Strategy for 3D Huygens' Principle Based Microwave Imaging

Bilal Khalid[1], **Banafsheh Khalesi**[1, 2, 3], **Navid Ghavami**[2, 3], **Giovanni Raspa**[2], **Mario Badia**[2], **Sandra Dudley**[1], **Mohammad Ghavami**[1], **and Gianluigi Tiberi**[1, 2, 3]

[1]School of Engineering, London South Bank University, London, UK
[2]Umbria Bioengineering Technologies, Perugia, Italy
[3]UBT UK Division, London, UK

Abstract— This paper focuses on executing a novel methodology to achieve imaging time reduction via 3D imaging algorithm based on Huygens principle using a microwave imaging device (MammoWave). Specifically, a three-layer cylindrical phantom with a 3D structured inclusion has been fabricated with varying dielectric properties. Various spiral-like (along z-axis) measurement scenarios have been considered to investigate the possibility of measurement time reduction. In the first scenario, we have performed measurements in spiral-like configuration-I at multiple planes along the z-axis, while for the second scenario we have applied spiral configuration-II in an alternate way in terms of receiving points. We found that the proposed spiral-like measurement scenarios may lead to a measurement time saving of 50%, with a lower S/C ratio (decrease of maximum 3.2 dB) and slightly higher error (approximately 3.5%) in inclusion dimensional analysis and localization.

1. INTRODUCTION

The ultra-wideband (UWB) technology has shown promising character and has developed immensely in the last decades by bringing conspicuous changes to our daily life, particularly in telecommunications and medical imaging. Imaging of the internal organs is currently very vital for detecting diseases providing timely cure. Microwave imaging (MWI) implies non-ionized and non-invasive short-time impulses at microwave frequencies making it an ideal candidate for medical imaging.

Over the last two decades, MWI has been widely employed as a novel diagnostic technique especially for breast cancer detection [1]. MWI has been exploited in detection of various diseases even at early stages such as brain strokes, bone fractures and skin cancer, as an alternative for conventional imaging technologies such as ultrasounds, X-rays, and magnetic resonance imaging [2]. MWI uses the non-ionized rays providing risk-free medical imaging and differentiates the healthy tissues and diseased tissues by differentiating the physical dielectric properties at the receiver's end [3]. MWI has been a hot topic for researchers to explore further applications of the technology, conspicuously 3-dimensional medical imaging as it would be very beneficial in determining the dimensions of the unhealthy parts.

In this paper, we have presented a novel 3D MWI technique based on Huygens principle (HP) applied using a fast MWI device named MammoWave [4]. Using HP based MWI methodology removes the requirement to solve inverse scattering and matrix inversions. Furthermore, it allows apprehending and combining the information from the individual frequencies, which in turn reconstructs a consistent image with localization having minimal error [5].

Recently a new 3D imaging technique based on HP via MammoWave has been presented in [6, 7] with successful 3D image reconstruction. Moreover, in [6] a detailed analysis of the reconstructed images has been performed such as dimensional analysis error and localization error calculations. Furthermore, measurements have been performed on six different cross-sections along the z-axis for 3D image reconstruction in [6] with each measurement taking 9–10 minutes. Although the proposed methodology in [6] is very successful in determining the various dimensions of the lesion along the z-axis, it takes time and further time reduction improvement is required.

In this paper, we have addressed the time reduction issue of [6] by introducing two scenarios, namely the spiral-like acquisition along the z-axis with different configurations. As testing case, we have fabricated a complex three-layer cylindrical phantom with 3D structured inclusion. Additionally, we have performed a detailed analysis of S/C ratio, dimensional error and localization

error corresponding to the proposed time saving approaches with two spiral-like acquisition configurations (configuration I & II). Along with these two spiral-like acquisition configurations we have tested one more configuration in order to test the possible achievable time reduction with minimal errors.

2. METHODOLOGY

2.1. Phantom Fabrication

In this paper, we have fabricated a complex phantom with three cylindrical layers and 3D structured spherical inclusion with varying dielectric properties. Specifically, the dedicated liquids were purchased from ZMT Zürich MedTech, Swiss, to fabricate the different cylindrical layers as shown in Table 1. The mixture containing 40% glycerol and 60% water possessing the dielectric properties shown in Table 1 has been used to fabricate the spherical 3D structured inclusion. In this proposed methodology, in order to have a more complex scenario, during the inclusion fabrication we have only filled the spherical part of the inclusion with the mixture leaving the rest of the tube empty.

Table 1: Dielectric properties of materials used in phantom fabrication.

Fabrication Materials	**Relative Permittivity (ε_r)**	**Conductivity (σ) [S/m]**
TLe11.5c.045oil (External layer)	7	0.3
TLe5c24 oil (Internal layer)	5	0.2
40% glycerol and 60% water	60	2

The cylinders mimicking the external and internal layers have diameters of 11 cm and 7 cm, respectively. The spherical inclusion's diameter at its tube-shaped cross-section is 1 cm and is 3.5 cm at its spherical cross-section. The fabricated spherical inclusion has been positioned in the internal cylindrical layer as shown in Fig. 1. Both cylinders are placed with a deviation of 3.5 cm between their centers.

Figure 1: The multilayered fabricated phantom with 3D structured inclusion.

2.2. Device and Imaging Procedure

In this paper, we have performed the measurements by acquiring the MWI device named MammoWave [4]. MammoWave comprises of a cylindrical hub made of aluminium, which is surrounded by two antennas Tx and Rx and microwave absorbers to cope with the free-space parameters. The device's operating frequency range is 1–6.5 GHz with the frequency sample size of 5 MHz and antennas rotating in 360° in the azimuth plane with the angular displacement of 4.5°. In the proposed 3D HP based imaging algorithm in [6, 7], we had performed the measurements at 6 planes along the z-axis on multiple fabricated phantoms by changing the height of the antennas simultaneously and reconstructing the 3D images. Moreover in [6, 7], we had measured the received signals S_{21} for every single plane along the z-axis by transmitting the signal at 5 central Tx planes (0°, 72°, 144°, 216°, 288°) with the angular shift of 4.5° and receiving the signals at 80 receiving points (from 0° to 360° at every 4.5°).

As the primary objective of this paper is to reduce measurement time, for that purpose we have performed spiral-like acquisition in two configurations by performing measurements at six planes along the z-axis by varying the height of both antennas i.e., $h_1, h_2, \ldots, h_6$. However, in the configuration-I instead of recording the received signal at 80 receiving points, we have recorded the signal utilizing first 40 Rx points for h_1, and for h_2 we have taken into consideration the Rx points from 41 to 80 and so on, the first 40 points for h_3, h_5 and second half for h_4, h_6 as shown in Fig. 2(a).

Moreover, for configuration-II we have recorded complex S_{21} by evaluating 40 Rx points with alternating 20 Rx points, specifically Rx points 1 to 20 and 40 to 60 for h_1, h_3, h_5, and Rx points 21 to 40 and 61 to 80 for h_2, h_4, h_6.

Furthermore, we have placed the fabricated phantom inside the cylindrical hub of the MammoWave and recorded measurements starting from the top (going downwards) at the multiple planes along the z-axis. The pictorial demonstration of the experimental setup and spiral-like configuration are shown in Fig. 2.

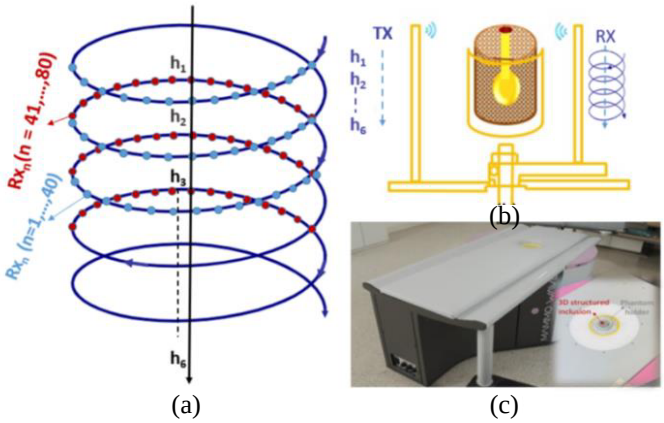

Figure 2: (a) Spiral-like acquisition configuration. (b) The experimental schematic. (c) MWI device MammoWave.

All the measurements have been performed in the frequency domain, as it is beneficial to combine the data from all the frequencies to reconstruct a consistent image.

The received signals at the multiple planes Z_h along the z-axis at different heights h_{n1} and h_{n2} can be represented as S_{21n1} and S_{21n2}:

$$\begin{aligned} S_{21n1} &= S_{21}{}^{m,p}_{n_1,h_{n1}}\left(a_0, \emptyset_{n_1}, Z_{h_{n1}}; Tx_{m,p,h_{n1}}; f\right) \\ S_{21n2} &= S_{21}{}^{m,p}_{n_2,h_{n2}}\left(a_0, \emptyset_{n_2}, Z_{h_{n2}}; \mathrm{Tx}_{m,p,h_{n2}}; f\right). \end{aligned}$$

where $n_1 = 1, \ldots, 40$ and $n_2 = 41, \ldots, 80$ indicate the receiving points representing spiral-like configuration-I and $n_1 = 1, \ldots, 20$ & $40, \ldots, 60$ and $n_2 = 21, \ldots, 40$ & $61, \ldots, 80$ for spiral-like configuration-II for heights $h_{n1} = h_1, h_3, h_5$ and $h_{n2} = h_2, h_4, h_6$ respectively for both configurations along the z-axis; $m = 1, \ldots, 5$ stipulates the central Tx points, $p = 1, 2, 3$ shows the positions of the transmitting points with the angular transposition of $\pm 4.5^\circ$ and f signifies the frequency.

These received signals are processed via Huygens' principle in order to remap the dielectric contrast of the internal field by calculating the external field; according to Huygens' principle, the calculated external field carries the information of the internal field, which can be presented as:

$$E^{\mathrm{rcstr}}_{\mathrm{HP,3D}}\left(\rho, \emptyset, Z; \mathrm{Tx}_{m,p,h_{n1}+h_{n2}}; f\right) = \sum_{h=1}^{h_{n1}} \sum_{h=2}^{h_{n1}} \sum_{n=1}^{n_1} \sum_{n=41}^{n_2} \left(S_{21n1} + S_{21n2}\right) G\left(k_1 \left|\overrightarrow{\rho_{n,h}} - \vec{\rho}\right|\right) \tag{1}$$

Hence, the intensity of the consistent 3D image can be obtained by summing all the solutions i.e., by gathering information from all the receiving points from spiral-like acquisitions along the z-axis for number of frequencies NF as shown below:

$$I_{3D}\left(\rho, \emptyset, Z; Tx_{m,p,h_{n1}+h_{n2}}\right) == \sum_{h=1}^{h_{n1}+h_{n2}} \sum_{i=1}^{NF} \left|E^{\mathrm{rcstr}}_{\mathrm{HP,3D}}\left(\rho, \emptyset, Z; \mathrm{Tx}_{m,p,h_{n1}+h_{n2}}; f\right)\right|^2 \tag{2}$$

Artefact removal has been performed using a rotation-subtraction procedure [6]. Finally, we have applied normalization with respect to the global maximum.

3. RESULTS AND DISCUSSIONS

3.1. Image Reconstruction

In this paper, we have performed two experiments by doing measurements at six planes along the z-axis. First, by applying spiral-like configuration-I i.e., considering Rx points 1–40 for h_1, h_3, h_5 and 41–80 for h_2, h_4, h_6 and then by measuring Rx points 1 to 20 and 40 to 60 for h_1, h_3, h_5, and Rx points 21 to 40 and 61 to 80 for h_2, h_4, h_6. Performing measurements using these methodologies has significantly reduced the acquisition time by 50%; we have also quantified the obtained results by various factors to calculate the difference compared to original setup.

As during the phantom fabrication, we only filled the spherical part of the 3D structured inclusion with the fabrication mixture, we aimed to detect the inclusion at the cross-section 5 and 6 i.e., at h_5, h_6 as shown in Fig. 3 [6].

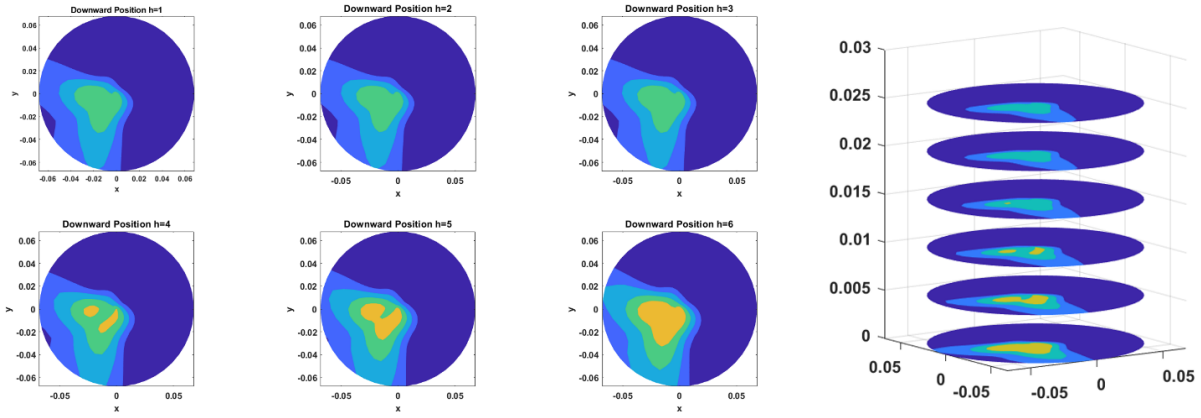

Figure 3: (a) Reconstructed microwave images with detected inclusion at reference planes (when employing all frequency points at each height). (b) 3D reconstructed image. Images are produced after normalization and image adjustment.

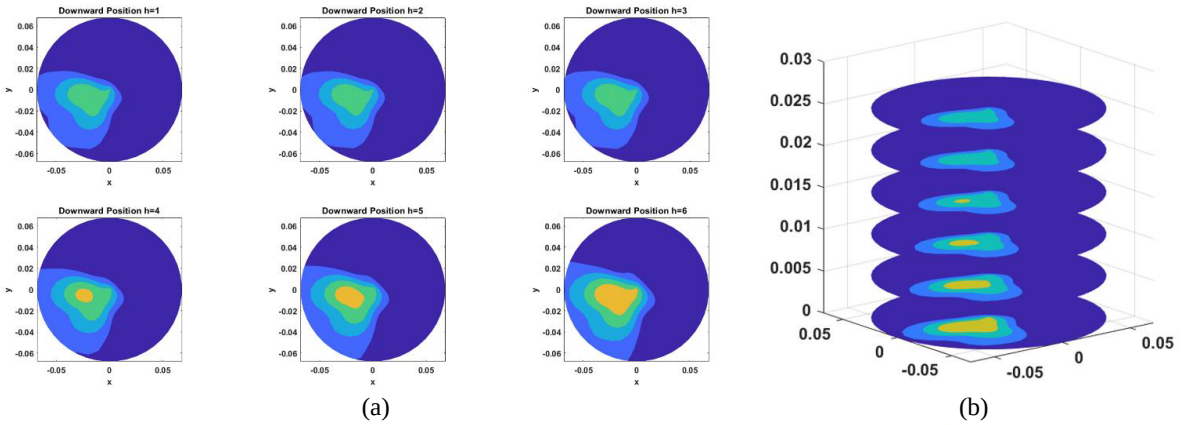

Figure 4: (a) Reconstructed microwave images with detected inclusion at reference planes (spiral-like acquisition Configuration-I). (b) 3D reconstructed image, Images are produced after normalization and image adjustment.

For the first scenario i.e., spiral-like acquisition configuration-I, the reconstructed images at multiple planes along the z-axis along with the 3D visualization are shown in Fig. 4. As we can

clearly see in Fig. 4(a) the images reconstructed at the heights h_5 and h_6 show the detected inclusion more prominently with the varying dimensions than the other planes. These results clearly indicate the successful implication of the spiral-like acquisition configuration with promising results.

For the second scenario i.e., spiral-like configuration-II, Fig. 5(a) shows the images reconstructed at multiple planes along the z-axis, and it clearly shows the detection at last two planes but with a dimensional error. Fig. 5(b) shows the corresponding 3D visualization of the detected inclusion, where the variation in dimensions of the inclusion can be observed.

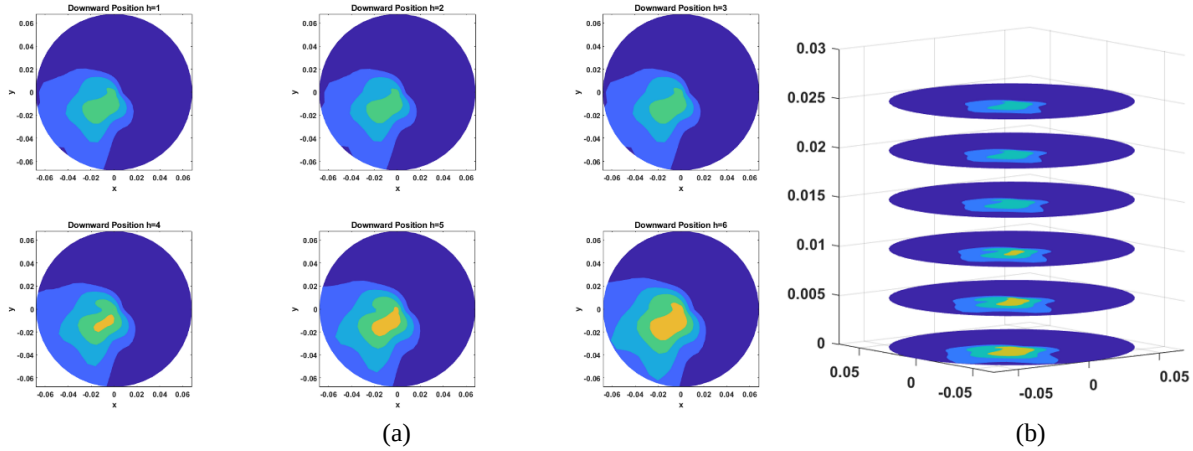

Figure 5: (a) Reconstructed microwave images with detected inclusion at reference planes (spiral-like acquisition configuration-II). (b) 3D reconstructed image. Images are produced after normalization and image adjustment.

3.2. Image Quantification

After generating the reconstructed images via 3D imaging algorithm, we have performed a detailed analysis for all three scenarios i.e., (i) the original setup as in [6], (ii) spiral-like acquisition configuration-I and (iii) spiral-like acquisition configuration-II. As per the experimental arrangement i.e., only spherical part of the inclusion was filled with fabrication mixture, we expected to detect the inclusion at h_4, h_5, h_6 and this was achieved as evident from Figs. 4 and 5.

In order to perform the analysis, we have taken into consideration the reconstructed images at heights h_4, h_5, h_6 along the z-axis. Fig. 6(a) shows the detected inclusion at h_4, h_5, h_6 for the original experimental setup and the red circles show the actual location of the inclusion aligning with the realistic scenario. Figs. 6(b) and (c) show the detected inclusion at h_4, h_5, h_6 for spiral-like acquisition configuration I & II respectively. The diameters of the red circles representing the actual size and location of the inclusion at multiple planes along the z-axis for Figs. 6(a), (b) and (c) are the same.

We have calculated the signal to clutter ratio (S/C) for all the three scenarios in order to perform a comparison at h_4, h_5, h_6 along the z-axis, as shown in in Table 2. The S/C is the ratio between maximum intensity evaluated in the region of the inclusion divided by the maximum intensity outside the region of the inclusion [9].

As it can be observed, for the spiral-like acquisition configuration-I the S/C ratio at h_6 (where the inclusion has its largest diameter) drops from 10.48 dB to 9.28 dB with the difference of 1.2 dB, however for the spiral-like configuration-II this ratio drops by 3.14 dB, compared to the original setup.

Furthermore, we have calculated the dimensional analysis error (as described in [6]) for all the three scenarios: Table 3 shows the dimensional error in percentage. Hence, it is clear from the values presented in Table 3 that there is an increased error percentage for the two proposed methodologies (for achieving the time reduction) as compared to original setup. For spiral-like acquisition configuration-I, the increase in error percentage ranges from 1.4% to 3.62%, while this increase in error is even higher for the spiral-like configuration-II, which is around 6%.

Moreover, we have also calculated the localization error (as described in [6]): from the values presented in Table 4 we can conclude that the localization error for spiral-like acquisition configuration-I is less than the spiral-like configuration-II.

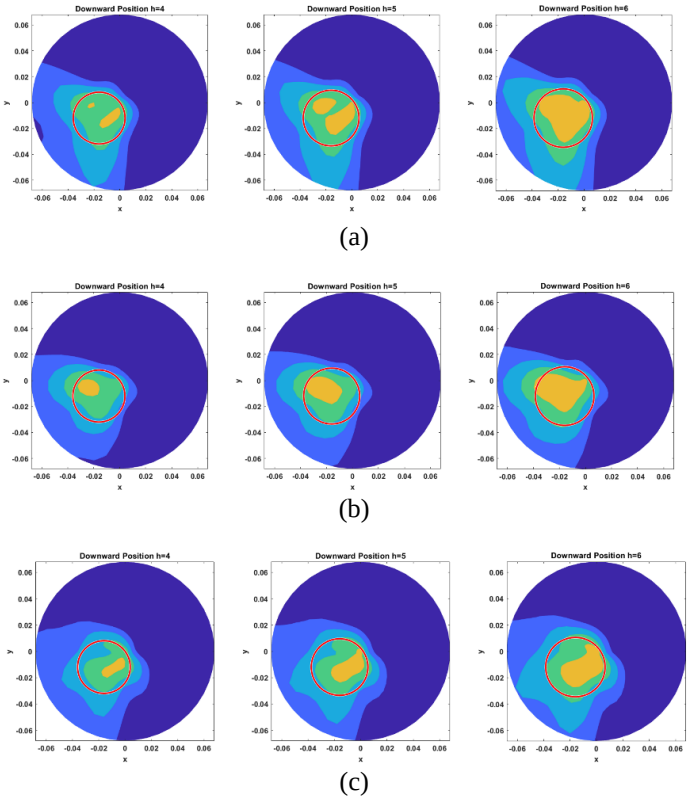

Figure 6: Reconstructed microwave images with detected inclusion at h_4, h_5, h_6 using: (a) original setup, (b) spiral-like acquisition configuration-I, (c) spiral-like acquisition configuration-II.

Table 2: Signal to Clutter (S/C) Ratio Comparison for all three scenarios.

Z_h along the z-axis	Signal to Clutter (S/C) Ratio (dB) Comparison		
	Original Setup	***Spiral-like Acquisition Configuration-I***	***Spiral-like Acquisition Configuration-II***
$h = 4$	4.99	4.59	2.56
$h = 5$	7.48	7.04	5.94
$h = 6$	10.48	9.28	7.34

Table 3: Dimensional Analysis Error Comparison for all three scenarios.

Z_h along the z-axis	Dimensional Analysis Error (%)		
	Original Setup	***Spiral-like Acquisition Configuration-I***	***Spiral-like Acquisition Configuration-II***
$h = 4$	10.69	11.92	14.98
$h = 5$	8.91	10.79	13.06
$h = 6$	6.04	9.66	11.78

In the original setup, the measurement time is 9 minutes per height; the configurations presented above achieved a measurement time reduction of approximately 50%. Following our analysis through several parameters, spiral-like acquisition configuration-I can be seen as the more suitable overall configuration out of the two.

Table 4: Localization Error Comparison for all three scenarios.

Z_h along the z-axis	Localization Error Calculation (mm)		
	Original Setup	***Spiral-like Acquisition Configuration-I***	***Spiral-like Acquisition Configuration-II***
$h = 4$	4.81	6.59	7.29
$h = 5$	3.56	5.13	6.07
$h = 6$	2.68	3.92	5.23

Beside these two configurations we have tested our methodology and imaging algorithm further to test the limit where we can achieve time reduction with minimum errors i.e., dimensional analysis error, localization error and S/C ratio analysis. For this purpose, we have reduced the Rx points to 1/3 for each z-plane, as compared to the previous configurations which used 40 Rx points. Specifically, we have implied the spiral configuration by taking into consideration Rx positions 1–27 for h_1, h_4, Rx positions 28–54 for h_2, h_5 and Rx positions 55–80 for h_3, h_6 utilizing one third of the receiving points at each plane along the z-axis. Fig. 7 shows the reconstructed images after using this spiral acquisition at multiple planes along the z-axis.

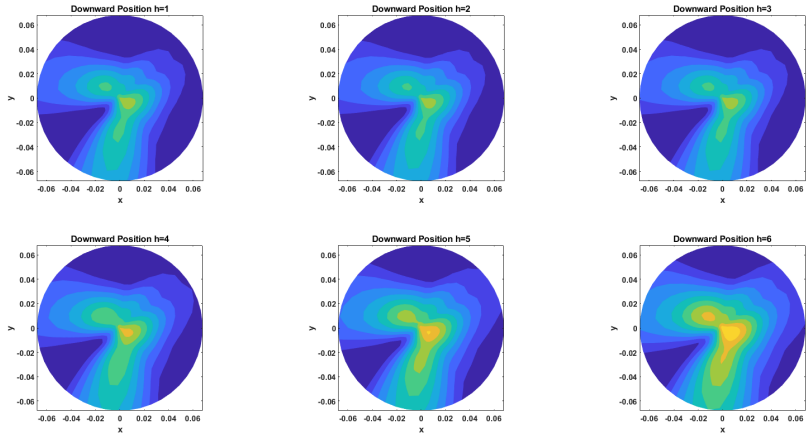

Figure 7: Reconstructed microwave images with detected inclusion at reference planes (spiral-like acquisition Configuration using 1/3 of Rx points).

As can be observed from the obtained images, our proposed methodology is not successful in this scenario. Specifically, considering $h = 6$ where the inclusion is at largest diameter the signal to clutter ratio drops by 6.5 dB as compared to the original setup and 4 dB as compared to spiral-like acquisition configuration-I. Similarly, we have applied other quantification parameters as well and have seen increased dimensional analysis error by 20% and localization error by 17 mm, which is significant. Hence reducing the number of Rx points to 1/3 would result in increased error percentages.

4. CONCLUSIONS

In this paper, we have investigated the applicability of a spiral-like acquisition strategy for 3D Huygens' Principle based microwave imaging for achieving the measurement time reduction. For this purpose, specifically, a three-layer cylindrical phantom with a 3D structured inclusion has been fabricated with varying dielectric properties. Spiral-like acquisition has been performed by considering two different configurations on the multiple planes along the z-axis. In the first scenario (configuration I), the signals have been recorded by utilizing the first 40 Rx points for h_1, and second 40 Rx points (from 41 to 80) for h_2 and so on, the first 40 points for h_3, h_5 and second half for h_4, h_6. In the second scenario (configuration II), the complex S_{21} have recorded by evaluating 40 Rx points with alternating 20 Rx points, specifically Rx points 1 to 20 and 40 to 60 for $h_(1), h_3, h_5$,

and Rx points 21 to 40 and 61 to 80 for h_2, h_4, h_6. Our findings indicate that both scenarios have the capability to achieve promising image reconstruction while reducing measurement time by 50%. Specifically, we found that a measurement time saving of 50% leads to a S/C ratio decreases of maximum 3.2 dB and to a slightly higher error (approximately 3.5%) in dimensional analysis and localization error. Finally, we examined the spiral-like acquisition by utilizing only one third of receiving points which led to further increase in the error percentages.

ACKNOWLEDGMENT

This work was supported in part by the European Union's Horizon 2020 research and innovation programme under grant agreement No. 830265 (project MammoWave-Cutting edge microwave imaging device for safe and accurate breast cancer screening); in part by the European Union's Horizon 2020 research and innovation programme under the Marie Sklodowska-Curie grant agreement No. 872752 (project ROVER- Reliable Technologies and Models for Verified Wireless Body-centric Transmission and Localisation); in part by the European Union's Horizon 2020 research and innovation programme under grant agreement No. 101017098 (project RadioSpin-Deep Oscillatory Neural Networks Computing and Learning through the Dynamics of RF Neurons Interconnected by RF Spintronic Synapses).

REFERENCES

1. Conceição, R. C., J. J. Mohr, and M. O'Halloran, eds., *An Introduction to Microwave Imaging for Breast Cancer Detection*, Springer International Publishing, Basel, Switzerland, 2016.
2. Lin, X., Y. Chen, Z. Gong, B. C. Seet, L. Huang, and Y. Lu. "Ultrawideband textile antenna for wearable microwave medical imaging applications," *IEEE Transactions on Antennas and Propagation*, Vol. 68, No. 6, 4238-4249, 2020.
3. Pastorino, M., and A. Randazzo, *Microwave Imaging Methods and Applications*, Artech House, 2018.
4. Vispa, A., L. Sani, M. Paoli, A. Bigotti, G. Raspa, N. Ghavami, S. Caschera, M. Ghavami, M. Duranti, and G. Tiberi, "UWB device for breast microwave imaging: Phantom and clinical validations," *Measurement*, Vol. 146, 582–589, 2019.
5. Ghavami, N., G. Tiberi, D. J. Edwards, and A. Monorchio, "UWB microwave imaging of objects with canonical shape," *IEEE Transactions on Antennas and Propagation*, Vol. 60, No. 1, 231–239, 2011.
6. Khalid, B., B. Khalesi, N. Ghavami, L. Sani, A. Vispa, M. Badia, S. Dudley, M. Ghavami, and G. Tiberi, "3D huygens principle based microwave imaging through mammowave device: Validation through phantoms," *IEEE Access*, Vol. 10, 106770–106780, 2022.
7. Khalid, B., B. Khalesi, N. Ghavami, S. Dudley, M. Ghavami, and G. Tiberi, "3D microwave imaging using huygens principle: A phantom-based validation," *2021 IEEE Photonics & Electromagnetics Research Symposium (PIERS)*, 2892–2896, November 2021.
8. Khalesi, B., B. Sohani, N. Ghavami, M. Ghavami, S. Dudley, and G. Tiberi, "Free-space operating microwave imaging device for bone lesion detection: A phantom investigation," *IEEE Antennas and Wireless Propagation Letters*, Vol. 19, No. 12, 2393–2397, 2020.
9. Khalesi, B., B. Sohani, N. Ghavami, M. Ghavami, S. Dudley, and G. Tiberi, "A phantom investigation to quantify Huygens principle based microwave imaging for bone lesion detection," *Electronics*, Vol. 8, No. 12, 1505, 2019.